COMPARATIVE ANALYSIS BETWEEN SYNCHRONOUS GENERATORS AND VIRTUAL SYNCHRONOUS MACHINE GRID-FORMING INVERTER

by

UEKAWA Vitor Eiti

A Master Thesis

Submitted to
the School of Engineering of Tokyo Institute of Technology
on January 23, 2024
for the Degree of Master of Science
in Systems and Control Engineering

ABSTRACT

Acknowledgements

Contents

1 Introduction **1**
1.1 Background 1
1.2 Objectives 3
1.3 Strcture of the Thesis 3

2 Overview of Main VSG Topologies **4**
2.1 VSYNC Project's VSG Topology 4
2.2 IEPE's VSG Topology 5
2.3 KHIs' VSG Topology 8
2.4 ISE Lab's VSG Topology 9
2.5 Synchronverter 10

Appendices **11**

A Synchronous Generators **12**
A.1 Modeling of Synchronous Generators 12
A.1.1 General Structure of Synchronous Generators 12
A.1.2 Linear Magnetic Circuit 14
A.1.3 Park's Transformation (*dq0*-transformation) 15
A.1.4 Per-Unit System 17
A.1.5 Park's Model (Detailed Model) 18
A.1.6 2-axis Model (Subtransient Model) 19
A.1.7 1-axis Model (Flux-Decay Model) 20
A.1.8 Classical Model 20
A.2 Modeling of Exciter and Automatic Voltage Regulator (AVR) . . 20
A.3 Modeling of Turbine/Governor 20
A.4 Power System Stabilizer (PSS) 20
A.5 Automatic Generation Control (AGC) 20

References **21**

Chapter 1

Introduction

1.1 Background

The growing demand for energy and the challenges related to climate change require a transition towards renewable-based generation. Some examples of environmental requirements are discussed in the Sustainable Development Goals (SDGs) [1] and the Conference of the Parties (COP) [2] by the United Nations. It has been established that global net human-caused emissions of carbon dioxide (CO_2) need to decrease by approximately 45 percent from 2010 levels by 2030, reaching net zero around 2050.

As a consequence, the total share of energy generation from renewable sources has been increasing significantly in recent years. Some studies predict that by 2050, 91% of electricity generation will come from renewable resources, primarily solar and wind energy [3]. These emerging sources come in various sizes, ranging from residential-scale rooftop systems to utility-scale power plants, and they are interconnected across the electric grid, linking both the distribution system and the high-voltage transmission system. Significantly, for the focus of our study, a considerable number of these new resources connect to the power system through power electronic inverters[4].

Therefore, the transition towards renewable-based generation implies a shift from large centralized generation units, mainly composed of synchronous generators (SG), to decentralized/distributed generation units, mainly composed of inverter-based resources (IBR).

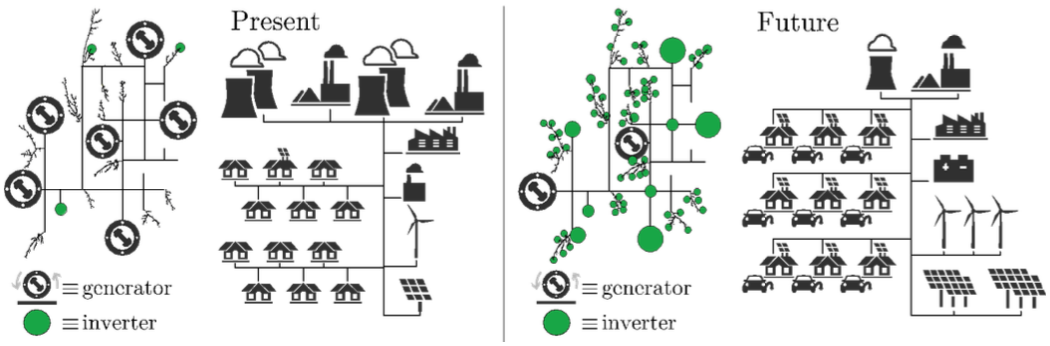

Figure 1.1: Present and future/projected power grids[4].

However, the replacement of SGs by IBRs has created new challenges for research related to stability requirements and the reliability and controllability of the system [5]. Some of the challenges include:

- Low inertia and frequency issues
- Fault Ride Through (FRT) capability issues
- Power quality issues
- Uncertainty issues

Among the several issues mentioned, the loss of system inertia is the most detrimental to the power system [5]. System inertia refers to the kinetic energy of all interconnected SGs of a power system [6]. In the case of a sudden increase in load or loss of generation, the kinetic energy stored in the SGs can bridge the gap between generation and consumption for a few seconds until a control action takes corrective measures. Since IBRs rely on electronic devices, they have very low or no inertia, and substituting SMs with IBRs would lead to a drastic reduction in the total system inertia.

In addition, today's IBRs generally rely on phase-locked loops (PLLs) to estimate the voltage angle at the inverter terminals, which is then used to control the inverter current output using vector control [7]. Therefore, these inverters "follow" the grid voltage and frequency, which are typically generated by SGs, and are called grid-following inverters (GFLI). Consequently, this control technique only works well in stiff AC grids with low frequency and voltage deviations.

In summary, the penetration of GFLI-based IBRs in power generation is very limited, as they have very low inertia and rely on a stiff AC grid. To address this problem, a new inverter control paradigm called grid-forming control has been developed. Grid-Forming Inverters (GFMI) act as ideal voltage sources actively controlling the magnitude of voltage and the frequency at the point of common coupling (PCC) [8].

Consequently, GFMI is expected to facilitate the development of scalable and decentralized AC power systems, wherein the voltages and frequency are controlled through the collaborative interactions among the grid-forming units. The subsequent figure elucidates the primary distinctions between GFMI and GFLI.

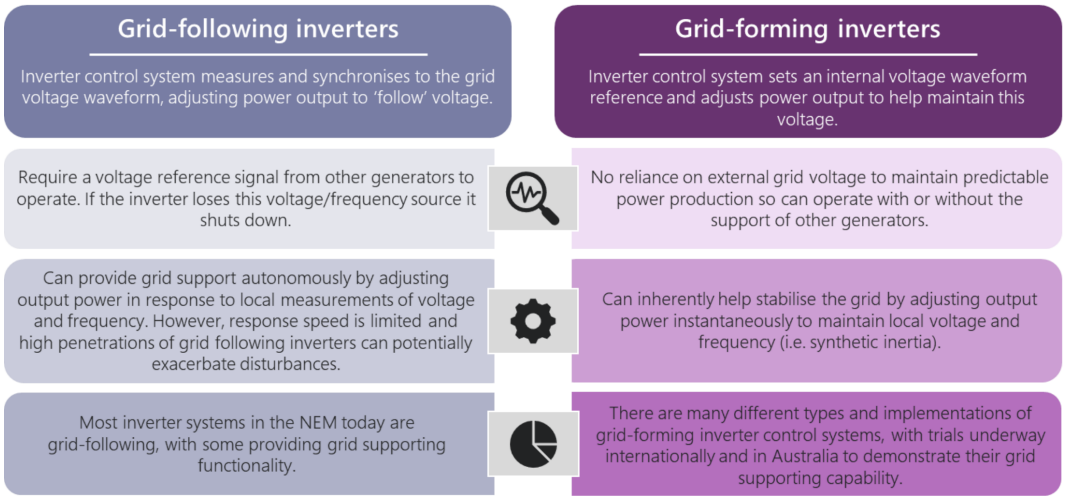

Figure 1.2: Differences between grid-following and grid-forming [9].

One of the most popular GFMI control approaches is based on introducing the SG dynamic models into the controllers of the inverter, enabling it to operate like a rotating electrical machine. This control approach is known as Virtual Synchronous Generator (VSG), and implementations of different orders have been reported in the literature, ranging from detailed electromechanical models [10][11] to simplified swing dynamics [12][13]. However, there is still little literature discussing the necessity of detailed electromechanical models, and models of intermediate complexity, such as the 1-axis (flux-decay) model, have not been reported yet [14].

1.2 Objectives

This thesis focuses on the modeling, simulation, and analysis of VSGs of different orders in a multi-machine power system with multiple SGs. The main goals of this project are to evaluate the necessity of detailed electromechanical models when implementing VSGs and to propose a VSG model equivalent to the 1-axis (flux-decay) SG model. The entire work is divided into the following steps:

1. Study of the modeling and simulation of voltage source power converters;
2. Study of the multiple implementations of VSGs;
3. Comparison between VSGs of multiple orders and 2-axis (subtransient) model of SG in terms of frequency deviation and output voltage and power under load increase and ground fault.

1.3 Strcture of the Thesis

The remainder of this thesis is organized as follows. In Chapter 2, we present an overview of the main implementations of VSGs in the literature, from detailed electromechanical models to simplified swing dynamics. In Chapter 3, we present a detailed mathematical modeling of voltage source converters, and their controllers enabling the VSGs dynamics. Chapter 4 presents the. In the Appendix, we describe the modeling and simulation methods of main power system components such as SMs, loads and transmission lines.

Chapter 2

Overview of Main VSG Topologies

With the increasing penetration of Inverter-Based Resources (IBRs) and the diminished involvement of Synchronous Generators (SGs) in energy generation, existing power systems are experiencing a loss of inertia. This loss significantly impacts two key aspects. Firstly, the absence of kinetic energy in the system leads to a higher frequency nadir and a faster rate of change in frequency (RoCoF), thereby affecting power quality and potentially causing the tripping of generators [13].

One of the most promising solutions to address these challenges is the implementation of Virtual Synchronous Generators (VSGs). A VSG is a control technique applied to the switching patterns of voltage source converters (VSCs), aiming to replicate the dynamic behavior of SGs.

Among the most notable research groups working on VSGs are: the VSYNC project [15] under the 6th European Research Framework program, the Virtual Synchronous Machine (VISMA) project [10] at the Institute of Electrical Power Engineering (IEPE) of Clausthal University of Technology in Germany, the VSG research team at Kawasaki Heavy Industries (KHIs) [16], and the Laboratory for Power Electronics and Electrical Drives (formerly ISE Lab) at Osaka University [13, 17, 18]. In this chapter, we provide an overview and comparison of the topologies developed by these research groups.

2.1 VSYNC Project's VSG Topology

The VSYNC project, initiated under the 6th European Research Framework program, represents a pioneering effort in implementing virtual inertia control for inverters. This project's system comprised an energy storage unit, a DC link, and a power inverter with an output LCL filter connected to an AC electrical grid [15].

The control scheme incorporates a Phase-Locked Loop (PLL) and a current reference generation circuit. The PLL is used for synchronization with the grid frequency and for providing an angle reference for the dq transformation. Meanwhile, the current reference generation circuit generates the reference current for controlling the inverter's switching pattern through PWM modulation. The overall control scheme of the VSYNC topology is illustrated in the following image.

The current reference is calculated based on the reference active P^* and reactive Q^* powers, which are calculated according to the SG swing equation so

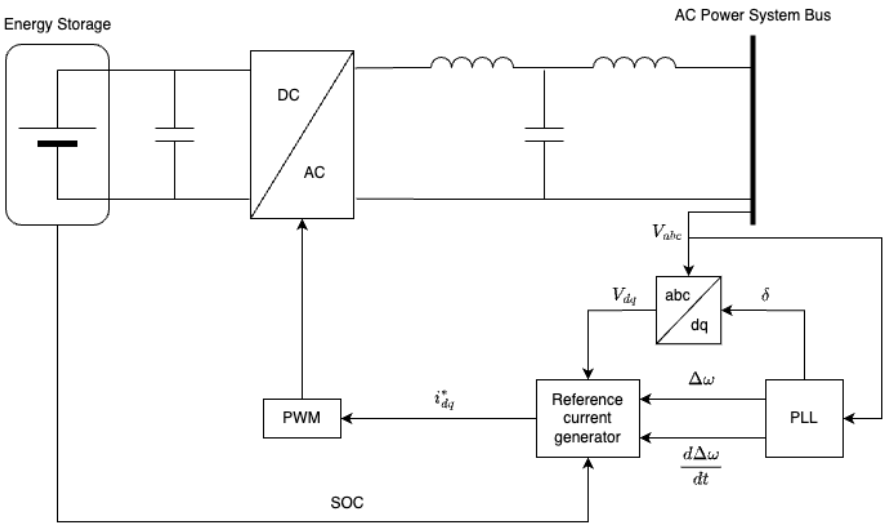

Figure 2.1: Overall control scheme of the VSYNC topology.

that the overall system can emulate the SGs inertial response.

$$P^* = K_{SOC}\Delta SOC + K_P\Delta\omega + K_t\frac{\Delta\omega}{dt}$$
$$Q^* = K_V\Delta V$$
$$i_d^* = \frac{V_dP^* - V_qQ^*}{(V_d + V_q)^2}$$
$$i_q^* = \frac{V_dQ^* - V_qP^*}{(V_d + V_q)^2}$$

Overall, the VSYNC control scheme is a current-source, grid-supporting control mechanism, employing a current control loop at the output terminal and using a PLL to detect grid frequency and provide an angle reference for the dq transformation. It is important to note that the use of a PLL can negatively impact control performance under weak AC systems. Furthermore, the VSYNC control scheme incorporates only the SG swing equation.

2.2 IEPE's VSG Topology

The IEPE group has proposed a VSG topology called Virtual Synchronous Machine (VISMA), which was first implemented as a current-source-based method on a hysteresis controlled inverter [10, 19], and later a voltage-source-based method was proposed to expand its applicability to PWM controlled inverters, which is more commonly used in the market [20]. The first is refered as VISMA-Method 1 and the second is refered as VISMA-Method 2 and their overall control scheme are illustrated in the following figures.

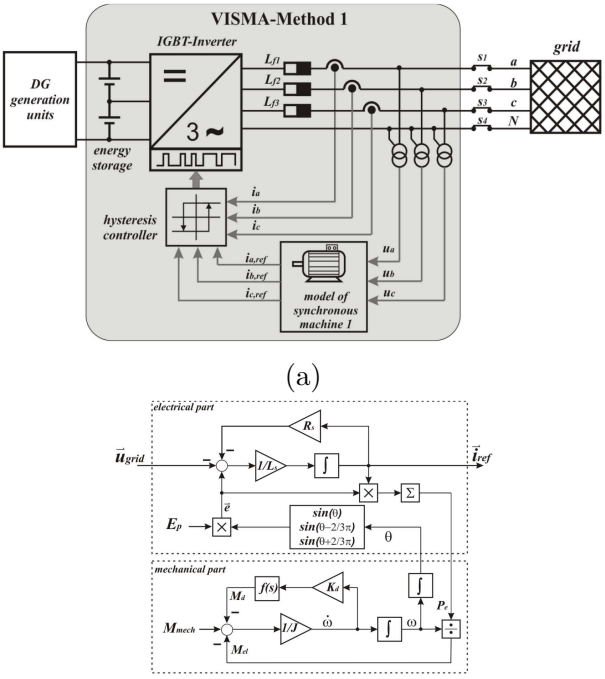

Figure 2.2: VISMA-Method 1 (current-source-based control) [20]. (a) Overall control scheme. (b) Model of synchronous machine 1.

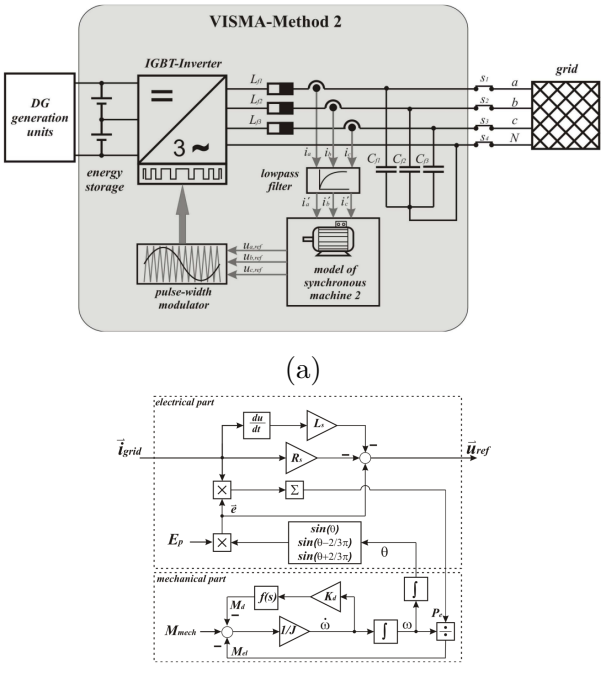

Figure 2.3: VISMA-Method 2 (voltage-source-based control) [20]. (a) Overall control scheme. (b) Model of synchronous machine 1.

The VISMA-Method 1 consists in measuring the grid voltage to feed the virtual synchronous machine algorithm, which outputs a reference current analogous to the stator current of a SG. The virtual synchronous machine algorithm consists of an electrical part and a mechanical part that interact with each other. The mechanical part corresponds to the rotor dynamics of the virtual synchronous machine, and can be represented by the following equations:

$$\begin{aligned} M_{mech} - M_{el} &= \frac{1}{J}\frac{d\omega}{dt} + k_d f(s)\frac{d\omega}{dt} \\ M_{el} &= \frac{P_{el}}{\omega} \\ \theta &= \int \omega dt \end{aligned}$$

where J is the moment of inertia, k_d is the mechanical damping factor, $f(s)$ is the phase compensation term, ω is the angular speed, θ is the angular position and M_{el} and M_{mech} are the electrical and mechanical torque.

M_{mech} represents the action of the virtual governor, which is simplified as being a control input to the system. The excitation system is also simplified, being represented by an adjustable amplitude E_p, resulting in the following induced electromotive force in the virtual stator.

$$\overrightarrow{e} = E_p \begin{bmatrix} e_a \\ e_b \\ e_c \end{bmatrix} = E_p \begin{bmatrix} \sin(\theta) \\ \sin(\theta - \frac{2\pi}{3}) \\ \sin(\theta + \frac{2\pi}{3}) \end{bmatrix}$$

Then, this induced electromotive force is used with the measured grid voltage in the electrical part of the virtual synchronous machine model to calculate the reference current, which is then used to drive the hysteresis controlled converter. The electrical part of the synchronous machine model is represented by the following equations.

$$\begin{aligned} e_a - u_a &= i_a^{ref} R_s + L_s \frac{di_a^{ref}}{dt} \\ e_b - u_b &= i_b^{ref} R_s + L_s \frac{di_b^{ref}}{dt} \\ e_c - u_c &= i_c^{ref} R_s + L_s \frac{di_c^{ref}}{dt} \end{aligned}$$

where (u_a, u_b, u_c) are the measured grid voltage in each line, R_s and L_s are the virtual stator resistance and inductance, respectively.

The working principle of the VISMA-Method 2 is exactly the same as of the VISMA-Method 1, with the exception that the grid current is used instead of the grid voltage for calculating the reference signal to drive the PWM based converter. In other words, the electrical part of the synchronous machine model is now represented by:

$$e_a - u_a^{ref} = i_a R_s + L_s \frac{di_a}{dt}$$
$$e_b - u_b^{ref} = i_b R_s + L_s \frac{di_b}{dt}$$
$$e_c - u_c^{ref} = i_c R_s + L_s \frac{di_c}{dt}$$

where (i_a, i_b, i_c) are the measured grid current in each line.

It is important to highlight that the VISMA topology does not require a PLL and uses a 5th order model of a SG, comprising of two mechanical state variables (*theta* and ω) and 3 electromagnetic state variables (the stator quantities). However, the damper and excitation windings are not taken into consideration, and the transient and sub-transient dynamics are ignored. Moreover, this model does not consider possible saliency effects of the rotor.

2.3 KHIs' VSG Topology

KHI has proposed a current-source-based VSG topology in the *dq*-coordinate frame[16], which control diagram is illustrated in the following image.

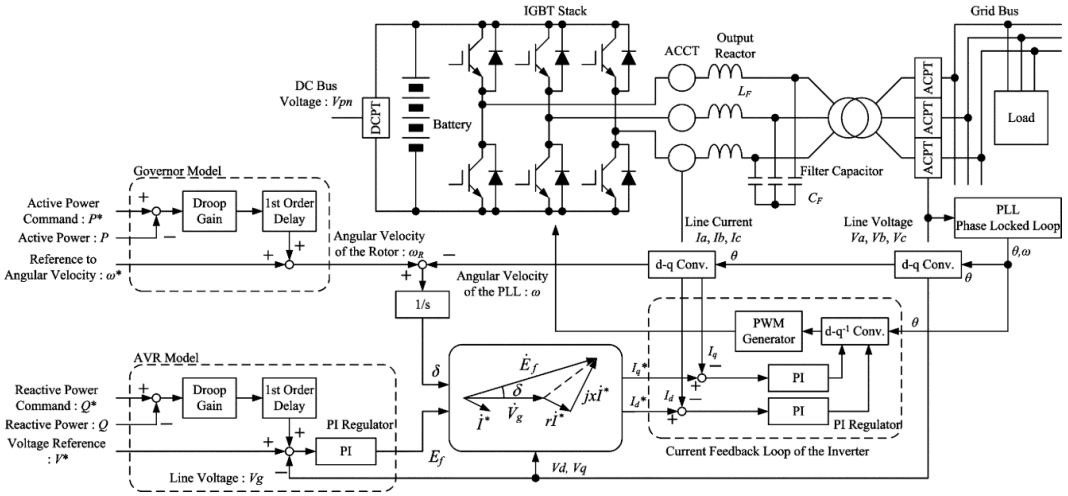

Figure 2.4: Control diagram of the VSG control developed by KHI[16].

In this model, the authors use phasor diagrams to express the relationship between the phase voltage and line currents of the virtual generator, thus ignoring the electrical dynamics. Moreover, the virtual generator is assumed to be cylindrical, with the same synchronous reactance on the direct and quadrature axes.

The model is composed of four main components: a PLL, an AVR, a virtual governor, a virtual generator model, and a current feedback loop. The PLL is used to detect the angular speed and angle of the grid side voltage of the inverter's output filter, which is used in the $dq-$transformations.

The output active and reactive powers are also measured, and they are in the virtual governor and AVR models to generate, respectively, the angular speed of the virtual rotor, and the internal electromotive force. The virtual governor and AVR models are simple PI controllers for active and reative power regulation.

The outputs from the virtual governor and AVR are then used to compute the reference current, which then passes through a current feedback loop to generate the reference signal for the PWM modulation.

2.4 ISE Lab's VSG Topology

The Laboratory for Power Electronics and Electrical Drives (formely ISE Lab) at Osaka University, which consists in emulating the SG swing equation [17, 21]. The following image describes the block diagram of the Ise Lab's VSG topology.

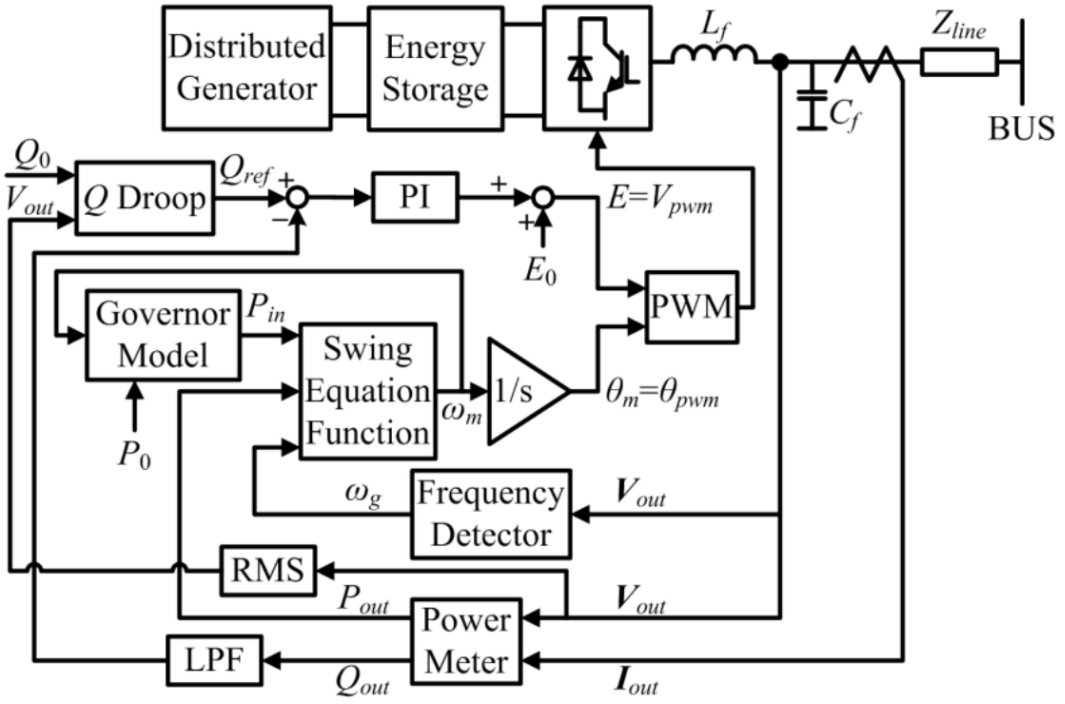

Figure 2.5: Control diagram of the VSG control developed by ISE Lab[22].

This model consists in measuring the output current and voltage, which are then used to compute the output active and reactive powers. The Frequency Detector block corresponds to a PLL that is used to measure the bus frequency ω_g which is used to compute the virtual rotor frequency through the swing equation:

$$P_{in} - P_{out} = J\omega_m \frac{d\omega_m}{dt} + D(\omega_m - \omega_g)$$

The rotor frequency is used as a reference for the governor model and the PWM inverter. Both the governor model and the Q Droop block are droop controllers creating linear droop control law between active power and frequency, and between reactive power and voltage, respectively.

It is important to highlight that no inner current or voltage loop is adopted in this control scheme, so that the filter reactance is analogous to the stator reactance of the VSG. Moreover, this VSG control can be classified as a voltage-source-based grid-forming control.

However,

2.5 Synchronverter

Appendices

Appendix A

Synchronous Generators

Synchronous generators form the backbone of contemporary power generation, converting the mechanical energy sourced from fossil fuel combustion or natural resources like water streams into electrical energy. Their operation at a constant speed synchronized with the AC power frequency has made them a staple in the field since the late 19th century.

This chapter delves into the enduring role of synchronous generators, focusing on their operational intricacies and control strategies. Over the years, various control methods, including Automatic Voltage Regulation (AVR), Power System Stabilization (PSS), and Automatic Generation Control (AGC), have been developed to ensure the stable performance of these machines.

The objective of this chapter is to elucidate key concepts and models associated with synchronous generators, providing a foundation for understanding their behavior. For a more detailed explanation in the modeling of synchronous generators, please refer to [23],[24] and [25].

A.1 Modeling of Synchronous Generators

A.1.1 General Structure of Synchronous Generators

A synchronous generator is mainly composed by a stator, in which three-phase windings are placed 120° apart in space, and a rotor, in which a field winding and three damper windings are placed. The field winding is connected to a DC current source, and the currents in the damper windings flow such that their magnetic fluxes are along the d- and q-axes, perpendicular to the rotor's axis.The following figure is a diagram of a three-phase synchronous generator.

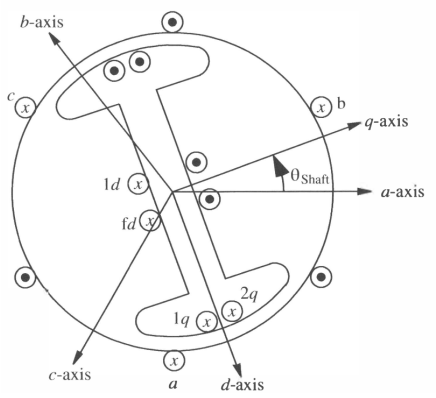

Figure A.1: Schematic diagram of a three-phase synchronous generator [23].

The assumptions made in the mathematical modeling of the synchronous generators are:

1. Stator windings are distributes sinusoidally along the air gap;
2. Stator slots do not cause any variation in the rotor inductances;
3. Magnetic hysteresis is negligible;
4. Magnetic circuit is considered linear.
5. The rotor has a single pair of poles.

Assumptions 1 to 3 are reasonable since the manufacturing process of synchronous machines is very precise. Assumption 4 is made for simplification, but in more complete analysis the nonlinearities of the magnetic circuit should be taken into account [26]. By applying the fundamental Kirchhoff's, Faraday's and Newton's laws, the following relationships can be derived.

$$\begin{cases} \frac{d\delta}{dt} = \omega_s \Delta\omega \\ M\frac{\Delta\omega}{dt} = -D\Delta\omega + P_m - P_e \\ v_a = -i_a r_s + \frac{d\lambda_a}{dt} \\ v_b = -i_b r_s + \frac{d\lambda_b}{dt} \\ v_c = -i_c r_s + \frac{d\lambda_c}{dt} \\ v_{fd} = i_{fd} r_{fd} + \frac{d\lambda_{fd}}{dt} \\ v_{1d} = i_{1d} r_{1d} + \frac{d\lambda_{1d}}{dt} \\ v_{1q} = i_{1q} r_{1q} + \frac{d\lambda_{1q}}{dt} \\ v_{2q} = i_{2q} r_{2q} + \frac{d\lambda_{2q}}{dt} \end{cases} \tag{A.1}$$

where v_i are the instantaneous phase to neutral voltage, i_i are the currents, r_i are the resistances and λ_i are the flux linkages in each phase i. Moreover, M is the inertia coefficient, D is the damping coefficient, P_m is the mehchanical torque applied to the shaft, P_e is the electrical torque, δ is the rotor angle θ_{shaft} relative to a rotating frame that rotates with constant speed equal to the synchronous speed ω_s, and $\Delta\omega = \omega - \omega_s$, where ω is the rotor's rotational speed.

A.1.2 Linear Magnetic Circuit

Considering the special case in which the magnetic circuit of the synchronous generator is linear in relation to the currents, the flux linkages can be expressed in the following matrix form [25]:

$$\begin{bmatrix}\lambda_a\\ \lambda_b\\ \lambda_c\end{bmatrix} = -\begin{bmatrix}l_{aa} & l_{ab} & l_{ac}\\ l_{ab} & l_{bb} & l_{bc}\\ l_{ac} & l_{bc} & l_{cc}\end{bmatrix}\begin{bmatrix}i_a\\ i_b\\ i_c\end{bmatrix} + \begin{bmatrix}l_{afd} & l_{a1d} & l_{a1q} & l_{a2q}\\ l_{afd} & l_{b1d} & l_{b1q} & l_{b2q}\\ l_{afd} & l_{b1d} & l_{c1q} & l_{c2q}\end{bmatrix}\begin{bmatrix}i_{fd}\\ i_{1d}\\ i_{1q}\\ i_{2q}\end{bmatrix} \tag{A.2}$$

$$\begin{bmatrix}\lambda_{fd}\\ \lambda_{1d}\\ \lambda_{1q}\\ \lambda_{2q}\end{bmatrix} = -\begin{bmatrix}l_{fda} & l_{fdb} & l_{fdc}\\ l_{1da} & l_{1db} & l_{1dc}\\ l_{1qa} & l_{1qb} & l_{1qc}\\ l_{2qa} & l_{2qb} & l_{2qc}\end{bmatrix}\begin{bmatrix}i_a\\ i_b\\ i_c\end{bmatrix} + \begin{bmatrix}l_{fdfd} & l_{fd1d} & 0 & 0\\ l_{1dfd} & l_{1d1d} & 0 & 0\\ 0 & 0 & l_{1q1q} & l_{1q2q}\\ 0 & 0 & l_{2q1q} & l_{2q2q}\end{bmatrix}\begin{bmatrix}i_{fd}\\ i_{1d}\\ i_{1q}\\ i_{2q}\end{bmatrix} \tag{A.3}$$

Note that the mutual inductances between the $d-$ and $q-$axes are zero, since they are perpendicular between each other. In normal operation, the angle between the windings in the rotor and in the stator are constanlty changing, thus the inductances vary according to the angle θ_{shaft}.

From definition, inductance is equal to the ratio of magnetic flux to current, magnetic flux is the product of permeance and magnetomotive force, and magnetomotive force is the product of of the current around the turns and the number of turns of a coil[27]. In other words:

$$\begin{aligned} l &= \frac{\lambda}{i}\\ \lambda &= N\phi,\\ \phi &= FP,\\ F &= Ni \end{aligned}$$

where ϕ is magnetic flux, N is the number of turns of the coil, P is the permeance and F is the magnetomotive force. In order to understand how the inductances vary according to θ_{shaft}, let us analyze the magnetomotive force (mmf) in the a-winding of Figure A.1. Let $F_a = N_a i_a$ be the mmf in the a-winding, it can be split in the $d-$ and $q-$axes as follows:

$$\begin{aligned} F_{ad} &= F_a \sin(\theta_{shaft})\\ F_{aq} &= F_a \cos(\theta_{shaft}) \end{aligned} \tag{A.4}$$

Let P_d and P_q be the permeances along the $d-$ and $q-$axes, respectively, the total flux is therefore:

$$\begin{aligned} \phi_{aa} &= F_{ad}P_d \sin(\theta_{shaft}) + F_{aq}P_q \cos(\theta_{shaft})\\ &= F_a P_d \sin^2(\theta_{shaft}) + F_a P_q \cos^2(\theta_{shaft})\\ &= N_a i_a \left(\frac{P_d(1-\cos(2\theta_{shaft}))}{2} + \frac{P_q(1+\cos(2\theta_{shaft}))}{2}\right)\\ &= N_a i_a \left(\frac{P_d+P_q}{2} - \frac{P_d-P_q}{2}\cos(2\theta_{shaft})\right) \end{aligned} \tag{A.5}$$

Thus, the self-inductance l_{aa} can be written as:

$$l_{aa} = l_{aa0} - l_{aap}\cos\left(2\theta_{shaft}\right)$$

where:

$$l_{aa0} = N_a^2\left(\frac{P_d + P_q}{2}\right) \text{ and } l_{aap} = N_a^2\left(\frac{P_d - P_q}{2}\right)$$

Repeating the same procedure for the other windings, the matrices in Equations A.2 and A.3 become:

$$\begin{aligned} L_{ss} &= \begin{bmatrix} l_{aa} & l_{ab} & l_{ac} \\ l_{ab} & l_{bb} & l_{bc} \\ l_{ac} & l_{bc} & l_{cc} \end{bmatrix} \\ &= \begin{bmatrix} l_{aa0} - l_{aap}\cos\left(2\theta_{shaft}\right) & -\frac{1}{2}l_{aa0} - l_{aap}\cos\left(2\theta_{shaft} - \frac{2\pi}{3}\right) & -\frac{1}{2}l_{aa0} - l_{aap}\cos\left(2\theta_{shaft} + \frac{2\pi}{3}\right) \\ -\frac{1}{2}l_{aa0} - l_{aap}\cos\left(2\theta_{shaft} - \frac{2\pi}{3}\right) & l_{aa0} - l_{aap}\cos\left(2\theta_{shaft} + \frac{2\pi}{3}\right) & -\frac{1}{2}l_{aa0} - l_{aap}\cos\left(2\theta_{shaft}\right) \\ -\frac{1}{2}l_{aa0} - l_{aap}\cos\left(2\theta_{shaft} + \frac{2\pi}{3}\right) & -\frac{1}{2}l_{aa0} - l_{aap}\cos\left(2\theta_{shaft}\right) & l_{aa0} - l_{aap}\cos\left(2\theta_{shaft} - \frac{2\pi}{3}\right) \end{bmatrix} \end{aligned}$$

$$\begin{aligned} L_{sr} &= \begin{bmatrix} l_{afd} & l_{a1d} & l_{a1q} & l_{a2q} \\ l_{afd} & l_{b1d} & l_{b1q} & l_{b2q} \\ l_{afd} & l_{b1d} & l_{c1q} & l_{c2q} \end{bmatrix} \\ &= \begin{bmatrix} l_{sfd}\sin(\theta_{shaft}) & l_{s1d}\sin(\theta_{shaft}) & l_{s1q}\cos(\theta_{shaft}) & l_{s2q}\cos(\theta_{shaft}) \\ l_{sfd}\sin(\theta_{shaft} - \frac{2\pi}{3}) & l_{s1d}\sin(\theta_{shaft} - \frac{2\pi}{3}) & l_{s1q}\cos(\theta_{shaft} - \frac{2\pi}{3}) & l_{s2q}\cos(\theta_{shaft} - \frac{2\pi}{3}) \\ l_{sfd}\sin(\theta_{shaft} + \frac{2\pi}{3}) & l_{s1d}\sin(\theta_{shaft} + \frac{2\pi}{3}) & l_{s1q}\cos(\theta_{shaft} + \frac{2\pi}{3}) & l_{s2q}\cos(\theta_{shaft} + \frac{2\pi}{3}) \end{bmatrix} \end{aligned}$$

where:

$$\begin{aligned} l_{afd} = l_{bfd} = l_{cfd} = l_{sfd} \\ l_{a1d} = l_{b1d} = l_{c1d} = l_{s1d} \\ l_{a1q} = l_{b1q} = l_{c1q} = l_{s1q} \\ l_{a2q} = l_{b2q} = l_{c2q} = l_{s2q} \end{aligned}$$

Since the above matrices vary with θ_{shaft}, it is convenient to make a coordinate transformation to a rotating reference system with same speed as θ_{shaft} so that the trigonometrical terms disappear. This coordinate transformation is referred to Park's transformation (or $dq0-$transformation) and drastically reduces the complexity of the equations.

A.1.3 Park's Transformation (*dq0*-transformation)

In power systems, the $dq0$-transformation, also known as Park's transformation, consists in converting from the static abc frame to a rotating $dq0$ frame. The main objective of this transformation is to reduce a three-phase sinusoidal components into two-dimensional DC components, and therefore it results in

relatively simple dynamic models that can be controlled through classical PID controllers.

This transformation slightly differs from author to author depending on the choice of the leading and lagging components. For instance, in [23] the authors consider the a-axis and the q-axis initially aligned, while in [24] the authors considers the a-axis and the d-axis initially aligned.

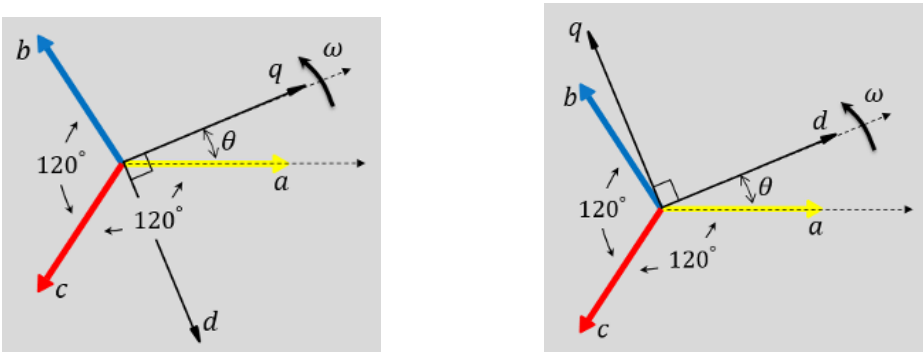

(a) The a-axis and the q-axis are initially aligned.

(b) The a-axis and the d-axis are initially aligned.

Figure A.2: Different representations of *dq0* frame.

In this thesis, the a-axis and the q-axis are chosen to be initially aligned. In this case, the Park transformation can be expressed by the following transformation matrix from *abc* frame to the rotating $dq0$ frame.

$$T_{dq0} = \frac{2}{3}\begin{bmatrix} \sin(\theta) & \sin\left(\theta - \frac{2\pi}{3}\right) & \sin\left(\theta + \frac{2\pi}{3}\right) \\ \cos(\theta) & \cos\left(\theta - \frac{2\pi}{3}\right) & \cos\left(\theta + \frac{2\pi}{3}\right) \\ \frac{1}{2} & \frac{1}{2} & \frac{1}{2} \end{bmatrix} \tag{A.6}$$

The inverse transformation can be expressed by the following matrix.

$$T_{dq0}^{-1} = \begin{bmatrix} \sin(\theta) & \cos(\theta) & 1 \\ \sin\left(\theta - \frac{2\pi}{3}\right) & \cos\left(\theta - \frac{2\pi}{3}\right) & 1 \\ \sin\left(\theta + \frac{2\pi}{3}\right) & \cos\left(\theta + \frac{2\pi}{3}\right) & 1 \end{bmatrix} \tag{A.7}$$

Applying this transformation to the stator voltages, i.e. the first three equations in Equation A.1:

$$\begin{aligned} \begin{bmatrix} v_d \\ v_q \\ v_0 \end{bmatrix} &= -T_{dq0}\begin{bmatrix} r_s & 0 & 0 \\ 0 & r_s & 0 \\ 0 & 0 & r_s \end{bmatrix} T_{dq0}^{-1}\begin{bmatrix} i_d \\ i_q \\ i_0 \end{bmatrix} + T_{dq0}\frac{d}{dt}\left(T_{dq0}^{-1}\begin{bmatrix} \lambda_d \\ \lambda_q \\ \lambda_0 \end{bmatrix}\right) \\ &= -\begin{bmatrix} r_s & 0 & 0 \\ 0 & r_s & 0 \\ 0 & 0 & r_s \end{bmatrix}\begin{bmatrix} i_d \\ i_q \\ i_0 \end{bmatrix} + T_{dq0}\frac{dT_{dq0}^{-1}}{dt}\left(\begin{bmatrix} \lambda_d \\ \lambda_q \\ \lambda_0 \end{bmatrix}\right) + \frac{d}{dt}\left(\begin{bmatrix} \lambda_d \\ \lambda_q \\ \lambda_0 \end{bmatrix}\right) \\ &= -\begin{bmatrix} r_s & 0 & 0 \\ 0 & r_s & 0 \\ 0 & 0 & r_s \end{bmatrix}\begin{bmatrix} i_d \\ i_q \\ i_0 \end{bmatrix} + \begin{bmatrix} 0 & -\omega & 0 \\ \omega & 0 & 0 \\ 0 & 0 & 0 \end{bmatrix}\begin{bmatrix} \lambda_d \\ \lambda_q \\ \lambda_0 \end{bmatrix} + \frac{d}{dt}\left(\begin{bmatrix} \lambda_d \\ \lambda_q \\ \lambda_0 \end{bmatrix}\right) \end{aligned}$$

Therefore, the Equation A.1 in the $dq0$ coordinates has the forms:

$$\begin{cases} \frac{d\delta}{dt} = \omega_s \Delta\omega \\ M\frac{\Delta\omega}{dt} = -D\Delta\omega + P_m - P_e \\ v_d = -r_s i_d - \omega\lambda_q + \frac{d\lambda_d}{dt} \\ v_q = -r_s i_q + \omega\lambda_d + \frac{d\lambda_q}{dt} \\ v_0 = -r_s i_0 + \frac{d\lambda_0}{dt} \\ 1v_{fd} = r_{fd} i_{fd} + \frac{d\lambda_{fd}}{dt} \\ v_{1d} = r_{1d} i_{1d} + \frac{d\lambda_{1d}}{dt} \\ v_{1q} = r_{1q} i_{1q} + \frac{d\lambda_{1q}}{dt} \\ v_{2q} = r_{2q} i_{2q} + \frac{d\lambda_{2q}}{dt} \end{cases} \tag{A.8}$$

Moreover, in order to calculate the stator fluxes in the $dq0$ coordinates, let us apply the transformations A.6 and A.7 to Equations A.2 and A.3. For the explicit calculation, please refer to [24].

$$\begin{aligned} \lambda_d &= -(l_{md} + l_{ls}) i_d + l_{sfd} i_{fd} + l_{s1d} i_{1d} \\ \lambda_q &= -(l_{mq} + l_{ls}) i_d + l_{s1q} i_{fd} + l_{s2q} i_{1d} \\ \lambda_0 &= -l_{ls} i_0 \\ \lambda_{fd} &= -\frac{3}{2} l_{sfd} i_d + l_{fdfd} i_{fd} + l_{fd1d} i_{1d} \\ \lambda_{1d} &= -\frac{3}{2} l_{s1d} i_d + l_{fd1d} i_{fd} + l_{1d1d} i_{1d} \\ \lambda_{1q} &= -\frac{3}{2} l_{s1q} i_q + l_{1q1q} i_{1q} + l_{1q2q} i_{2q} \\ \lambda_{2q} &= -\frac{3}{2} l_{s2q} i_q + l_{1q2q} i_{1q} + l_{2q2q} i_{2q} \end{aligned} \tag{A.9}$$

where l_{md}, l_{mq} and l_{ls} are, respectively, the mutual inductance in the $d-$ and $q-$axes and the leakage inductance.

A.1.4 Per-Unit System

In power system studies, it is customary to scale all quantities using the per-unit system. Typically, voltage and power are selected based on the equipment ratings, and base values such as current and impedance are derived from these. When studying a system, a convenient round number, such as 100 MVA, is often chosen as the base power, and the base voltage is usually set to the nominal rated value of the system. The key advantages of employing a per-unit system include:

- **Ease of comparison:** the per-unit system eliminates differences in power and voltage drops across a circuit, allowing for the comparison of losses and performance among different equipment based on their impedances in per units.
- **Simplification of circuits with transformers:** in power systems with transformers, converting a transformer into its equivalent circuit on either the primary or secondary side is necessary. However, using per-unit systems makes the impedances referred to either side of a transformer identical, eliminating the need to calculate impedances on both sides.

- **Elimination of multiple voltage levels:** in power systems with multiple transformers, the per-unit system reduces all voltage levels to a single level, simplifying calculations by referencing all impedances to this level.
- **Elimination of $\sqrt{3}$ in three-phase circuits:** Per-unit systems eliminate the need for the $\sqrt{3}$ factor in three-phase systems, avoiding errors and simplifying calculations that involve per-phase and line-to-line conversions.

Due to the composition of multiple coils in its stator and rotor, a synchronous generator can be treated as multiple transformers, each with different voltage levels. Therefore, the use of a per-unit system is highly beneficial for analyzing synchronous generators, ensuring that rotor and stator quantities are referred to the same base.

In the subsequent subsections, Equations A.8 and A.9 are reformulated in the per-unit system, giving rise to the Park's model of a synchronous generator, also known as the detailed model. Subject to certain assumptions, this detailed model will be further reduced into the 2-axis, 1-axis, and classical models of a synchronous generator. For a detailed explanation of the reformulation of Equations A.8 and A.9 in the per-unit system, please refer to [23] and [25].

A.1.5 Park's Model (Detailed Model)

The Park's model, also known as the detailed model, corresponds to Equations A.8 and A.9 reformulated in the per-unit system. It represents a 9th-order system comprising 2 mechanical equations describing rotor motion and 7 electromechanical equations describing the three stator windings and four rotor windings (one field winding, and one damper winding on the d-axis, and two damper windings on the q-axis).

$$
\begin{cases}
\frac{d\delta}{dt} & = \omega_s \Delta\omega \\
M\frac{\Delta\omega}{dt} & = -D\Delta\omega + P_m - P_e \\
\frac{1}{\omega_s}\frac{d\psi_d}{dt} & = R_s I_d + \frac{\omega}{\omega_s}\psi_q + V_d \\
\frac{1}{\omega_s}\frac{d\psi_q}{dt} & = R_s I_q - \frac{\omega}{\omega_s}\psi_d + V_q \\
\frac{1}{\omega_s}\frac{d\psi_0}{dt} & = R_s I_0 + V_0 \\
T'_{do}\frac{dE_q}{dt} & = -E_q - (X_d - X'_d)\Big(I_d - \frac{(X'_d - X''_d)}{(X'_d - X_{ls})^2}(\psi_{1d} + \\
 & + (X'_d - X_{ls})I_d - E_q) + E_{fd} \\
T''_{do}\frac{d\psi_{1d}}{dt} & = -\psi_{1d} + E_q - (X'_d - X_{ls})I_d \\
T'_{qo}\frac{dE_d}{dt} & = -E_d - (X_q - X'_q)\Big(I_q - \frac{(X'_q - X''_q)}{(X'_q - X_{ls})^2}(\psi_{2q} + \\
 & + (X'_q - X_{ls})I_q + E_d\Big) \\
T''_{qo}\frac{d\psi_{2q}}{dt} & = -\psi_{2q} - E_d - (X'_q - X_{ls})I_q \\
\psi_d & = -X''_d I_d + \frac{(X''_d - X_{ls})}{(X'_d - X_{ls})}E_q + \frac{(X'_d - X''_d)}{(X'_d - X_{ls})}\psi_{1d} \\
\psi_q & = -X''_q I_q - \frac{(X''_q - X_{ls})}{(X'_q - X_{ls})}E_d + \frac{(X'_q - X''_q)}{(X'_q - X_{ls})}\psi_{2q} \\
\psi_0 & = -X_{ls} I_0
\end{cases}
\tag{A.10}
$$

A.1.6 2-axis Model (Subtransient Model)

The Park's model can be reduced to a 4th-order system, also known as the 2-axis model (or subtransient model), by eliminating the stator/network transients and assuming that the short-circuit time constants T''_{do} and T''_{qo} are sufficiently small [23].

First, the stator/network transients can be eliminated by assuming that ω_s is large enough such that $\frac{1}{\omega_s} \approx 0$. Then, the stator/network fluxes in Equation A.10 become.

$$\begin{cases} 0 & = R_s I_d + \frac{\omega}{\omega_s}\psi_q + V_d \\ 0 & = R_s I_q - \frac{\omega}{\omega_s}\psi_d + V_q \\ 0 & = R_s I_0 + V_0 \\ \psi_d & = -X''_d I_d + \frac{(X''_d - X_{ls})}{(X'_d - X_{ls})} E_q + \frac{(X'_d - X''_d)}{(X'_d - X_{ls})}\psi_{1d} \\ \psi_q & = -X''_q I_q - \frac{(X''_q - X_{ls})}{(X'_q - X_{ls})} E_d + \frac{(X'_q - X''_q)}{(X'_q - X_{ls})}\psi_{2q} \\ \psi_0 & = -X_{ls} I_0 \end{cases}$$

The solution of the above equations of ψ_0 and I_0 is trivial, and ψ_d and ψ_q can be eliminated, leaving only the following two equations to be solved for I_d and I_q.

$$\begin{cases} 0 & = R_s I_d - X''_q I_q - \frac{(X''_q - X_{ls})}{(X'_q - X_{ls})} E_d + \frac{(X'_q - X''_q)}{(X'_q - X_{ls})}\psi_{2q} + V_d \\ 0 & = R_s I_q - X''_d I_d - \frac{(X''_d - X_{ls})}{(X'_d - X_{ls})} E_q - \frac{(X'_d - X''_d)}{(X'_d - X_{ls})}\psi_{1d} + V_q \end{cases} \tag{A.11}$$

Moreover, assuming that the short-circuit time constants T''_{do} and T''_{qo} are sufficiently small, the damping winding dynamic equations in Equation A.10 become:

$$\begin{cases} 0 & = -\psi_{1d} + E_q - (X'_d - X_{ls}) I_d \\ 0 & = -\psi_{2q} - E_d - (X'_q - X_{ls}) I_q \end{cases}$$

Replacing ψ_{1d} and ψ_{2q} in Equation A.11:

$$\begin{cases} 0 & = R_s I_d - X'_q I_q - E_d + V_d \\ 0 & = R_s I_q + X'_d I_d - E_q + V_q \end{cases}$$

Finally, the Park's model is reduced to the two-axis model, also known as substransient model, and it is expressed by the following set of dynamical equations.

$$\begin{cases} \frac{d\delta}{dt} & = \omega_s \Delta\omega \\ M\frac{\Delta\omega}{dt} & = -D\Delta\omega + P_m - P_e \\ T'_{do}\frac{E_q}{dt} & = -E_q - (X_d - X'_d) I_d + E_{fd} \\ T'_{qo}\frac{E_d}{dt} & = -E_d + (X_q - X'_q) I_q \\ 0 & = R_s I_d - X'_q I_q - E_d + V_d \\ 0 & = R_s I_q + X'_d I_d - E_q + V_q \end{cases} \tag{A.12}$$

A.1.7 1-axis Model (Flux-Decay Model)

The 2-axis model still considers the dynamics of the damper winding $1q$ illustrated in Figure A.1. Similarly to the approximation made for eliminating the damper windings $1d$ and $2q$ in the previous subsection, if T'_{qo} is sufficiently small, the dynamic equation of the damper winding $1q$ becomes:

$$0 = -E_d + (X_q - X'_q)I_q$$

Replacing E_d in the algebraic equations for I_d and I_q, the model described by Equation A.12 becomes:

$$\begin{cases} \frac{d\delta}{dt} & = \omega_s \Delta\omega \\ M\frac{\Delta\omega}{dt} & = -D\Delta\omega + P_m - P_e \\ T'_{do}\frac{E_q}{dt} & = -E_q - (X_d - X'_d)I_d + E_{fd} \\ 0 & = R_s I_d - X_q I_q + V_d \\ 0 & = R_s I_q + X'_d I_d - E_q + V_q \end{cases} \tag{A.13}$$

which is often called the 1-axis (or flux-decay) synchronous machine model.

A.1.8 Classical Model

Finally, the classical model is a further simplification considering T'_{do} sufficiently small, and therefore the dynamic equation of the excitation winding can be ignored in the similar way as in the previous two subsections. In other words, the classical model only considers the mechanical dynamics of the synchronous generator, and can be described by the following set of equations.

$$\begin{cases} \frac{d\delta}{dt} & = \omega_s \Delta\omega \\ M\frac{\Delta\omega}{dt} & = -D\Delta\omega + P_m - P_e \\ 0 & = R_s I_d - X_q I_q + V_d \\ 0 & = R_s I_q + X_d I_d + V_q \end{cases} \tag{A.14}$$

A.2 Modeling of Exciter and Automatic Voltage Regulator (AVR)

A.3 Modeling of Turbine/Governor

A.4 Power System Stabilizer (PSS)

A.5 Automatic Generation Control (AGC)

References

[1] U. Nations, "The 17 sustainable development goals." URL: https://sdgs.un.org/goals, 2015.

[2] U. Nations, "Conference of the parties." URL: https://unfccc.int/process/bodies/supreme-bodies/conference-of-the-parties-cop.

[3] I. R. E. A. (IRENA), "World energy transitions outlook 2023: 1.5°c pathway," 2023.

[4] Y. Lin, J. H. Eto, B. B. Johnson, J. D. Flicker, R. H. Lasseter, H. N. Villegas Pico, G.-S. Seo, B. J. Pierre, and A. Ellis, "Research roadmap on grid-forming inverters," tech. rep., National Renewable Energy Lab.(NREL), Golden, CO (United States), 11 2020.

[5] M. S. Alam, F. S. Al-Ismail, A. Salem, and M. A. Abido, "High-level penetration of renewable energy sources into grid utility: Challenges and solutions," *IEEE Access*, vol. 8, pp. 190277–190299, 2020.

[6] P. Denholm, T. Mai, R. W. Kenyon, B. Kroposki, and M. O'Malley, "Inertia and the power grid: A guide without the spin," tech. rep., National Renewable Energy Lab.(NREL), Golden, CO (United States), 2020.

[7] M. Ndreko, S. Rüberg, and W. Winter, "Grid forming control for stable power systems with up to 100% inverter based generation: a paradigm scenario using the ieee 118-bus system," in *Proceedings of the 17th International Wind Integration Workshop, Stockholm, Sweden*, pp. 16–18, 2018.

[8] D. Pattabiraman, R. H. Lasseter., and T. M. Jahns, "Comparison of grid following and grid forming control for a high inverter penetration power system," in *2018 IEEE Power & Energy Society General Meeting (PESGM)*, pp. 1–5, 2018.

[9] E. Taylor, "Application of advanced grid-scale inverters in the nem," tech. rep., Australian Energy Market Operator, 2021.

[10] H.-P. Beck and R. Hesse, "Virtual synchronous machine," in *2007 9th International Conference on Electrical Power Quality and Utilisation*, pp. 1–6, 2007.

[11] C.-H. Zhang, Q.-C. Zhong, J.-S. Meng, X. Chen, Q. Huang, S.-h. Chen, and Z.-p. Lv, "An improved synchronverter model and its dynamic behaviour comparison with synchronous generator," in *2nd IET Renewable Power Generation Conference (RPG 2013)*, pp. 1–4, 2013.

[12] Q.-C. Zhong and G. Weiss, "Synchronverters: Inverters that mimic synchronous generators," *IEEE Transactions on Industrial Electronics*, vol. 58, no. 4, pp. 1259–1267, 2011.

[13] J. Alipoor, Y. Miura, and T. Ise, "Power system stabilization using virtual synchronous generator with alternating moment of inertia," *IEEE Journal of Emerging and Selected Topics in Power Electronics*, vol. 3, no. 2, pp. 451–458, 2015.

[14] M. Chen, D. Zhou, and F. Blaabjerg, "Modelling, implementation, and assessment of virtual synchronous generator in power systems," *Journal of Modern Power Systems and Clean Energy*, vol. 8, no. 3, pp. 399–411, 2020.

[15] J. Driesen and K. Visscher, "Virtual synchronous generators," in *2008 IEEE Power and Energy Society General Meeting - Conversion and Delivery of Electrical Energy in the 21st Century*, pp. 1–3, 2008.

[16] Y. Hirase, K. Abe, K. Sugimoto, and Y. Shindo, "A grid-connected inverter with virtual synchronous generator model of algebraic type," *Electrical Engineering in Japan*, vol. 184, no. 4, pp. 10–21, 2013.

[17] K. Sakimoto, Y. Miura, and T. Ise, "Stabilization of a power system with a distributed generator by a virtual synchronous generator function," in *8th International Conference on Power Electronics - ECCE Asia*, pp. 1498–1505, 2011.

[18] J. Liu, Y. Miura, H. Bevrani, and T. Ise, "Enhanced virtual synchronous generator control for parallel inverters in microgrids," *IEEE Transactions on Smart Grid*, vol. 8, no. 5, pp. 2268–2277, 2017.

[19] Y. Chen, R. Hesse, D. Turschner, and H.-P. Beck, "Improving the grid power quality using virtual synchronous machines," in *2011 international conference on power engineering, energy and electrical drives*, pp. 1–6, IEEE, 2011.

[20] Y. Chen, R. Hesse, D. Turschner, and H.-P. Beck, "Comparison of methods for implementing virtual synchronous machine on inverters," in *International conference on renewable energies and power quality*, vol. 1, 2012.

[21] T. Shintai, Y. Miura, and T. Ise, "Reactive power control for load sharing with virtual synchronous generator control," in *Proceedings of The 7th International Power Electronics and Motion Control Conference*, vol. 2, pp. 846–853, 2012.

[22] J. Liu, *Studies on Improving Dynamic Performance of Microgrids by Applying Virtual Synchronous Generator Control to Distributed Generators*. PhD thesis, Osaka University, 2016.

[23] P. W. Sauer, M. A. Pai, and J. H. Chow, *Power system dynamics and stability: with synchrophasor measurement and power system toolbox*. John Wiley & Sons, 2017.

[24] P. C. Krause, O. Wasynczuk, S. D. Sudhoff, and S. Pekarek, *Analysis of electric machinery and drive systems*, vol. 2. Wiley Online Library, 2002.

[25] S. Sivasubramani, "Synchronous machine modeling." URL: `https://www.iitp.ac.in/~siva/2022/ee549/Synchronous_Machine_Modelling.pdf`, 2022.

[26] P. S. Kundur and O. P. Malik, *Power System Stability and Control*. McGraw Hill, 2022.

[27] E. M. Purcell and D. J. Morin, *Electricity and Magnetism*. Cambridge University Press, 2013.